PCCP

PAPER

View Article Online
View Journal | View Issue

Cite this: *Phys. Chem. Chem. Phys.*, 2019, **21**, 17190

Ground-state charge-transfer interactions in donor:acceptor pairs of organic semiconductors – a spectroscopic study of two representative systems†

Giuliano Duva, *[a] Paul Beyer,‡[b] Reinhard Scholz,[c] Valentina Belova, §[a] Andreas Opitz,[b] Alexander Hinderhofer,[a] Alexander Gerlach[a] and Frank Schreiber[ad]

We investigate blended donor:acceptor (D:A) thin films of the two donors diindenoperylene (DIP) and poly(3-hexylthiophene) (P3HT) mixed with the strong acceptor 1,3,4,5,7,8-hexafluorotetracyanonaphthoquinodimethane (F_6TCNNQ) using Polarization-Modulation Infrared Reflection-Absorption Spectroscopy (PMIRRAS). For DIP:F_6TCNNQ thin films we first carry out a comprehensive study of the structure as a function of the D : A mixing ratio, which guides the analysis of the PMIRRAS spectra. In particular, from the red-shift of the nitrile (C≡N) stretching of F_6TCNNQ in the different mixtures with DIP, we quantify the average ground-state charge-transfer (GS-CT) to be ρ_{avg} = (0.84 ± 0.04) *e*. The PMIRRAS data for P3HT:F_6TCNNQ blended films reveal nearly the same shift of the CT-affected C≡N stretching peak for this system. This points towards a very similar CT strength for the two systems. We extend the analysis to the relative intensity of the C≡N to the C=C stretching modes of F_6TCNNQ in the mixtures with DIP and P3HT, respectively, and support it with DFT calculations for the isolated F_6TCNNQ. Such comparison allows to identify the vibrational signatures of the acceptor mono-anion in P3HT:F_6TCNNQ, thus indicating a much stronger, integer CT-type interactions for this system, in agreement with available optical spectroscopy data. Our findings stress the importance of a simultaneous analysis of C≡N and C=C stretching vibrations in F_6TCNNQ, or similar quinoid systems, for a reliable picture of the nature of GS-CT interactions.

Received 24th May 2019,
Accepted 23rd July 2019

DOI: 10.1039/c9cp02939g

rsc.li/pccp

1 Introduction

Organic semiconductors (OSCs) can be divided into two categories: polymers and small molecules. For both material classes, molecular doping has been realized, namely, admixture of small percentages of a molecular material to the host matrix (typically not more than 10% in molar ratio) in order to increase the electrical conductivity.[1] Knowledge of the details of intermolecular interactions allows therefore to design and choose suitable material combinations in order to achieve the desired doping efficiency.[2]

With molecular electrical doping, the molar ratio between the host material and the dopant is relatively high, therefore the theoretical number of donor:acceptor (D:A) complexes possibly forming is correspondingly small. A possibility to increase the number of D:A complexes in order to study, for instance, weak spectroscopic effects, is to employ a so-called bulk heterojunction architecture[6] blending two molecular materials in a ratio close to equimolarity. In this case, the number of D:A complexes that can possibly form is maximized. Such an architecture usually has a strong effect on the optical

[a] *University of Tübingen, Institute for Applied Physics, Auf der Morgenstelle 10, 72076 Tübingen, Germany. E-mail: giuliano.duva@uni-tuebingen.de*
[b] *Humboldt-Universität zu Berlin, Department of Physics, Newtonstraße 15, 12489 Berlin, Germany*
[c] *Dresden Integrated Center for Applied Physics and Photonic Materials, Nöthnitzer Str. 61, 01187 Dresden, Germany*
[d] *Center for Light-Matter Interactions, Sensors & Analytics (LISA⁺), Auf der Morgenstelle 15, 72076 Tübingen, Germany*

† Electronic supplementary information (ESI) available: Additional information on the preparation and characterization of the SiO_x layers on Au *via* Plasma-Enhanced Chemical Vapor Deposition (PECVD); AFM height-profiles and lock-in phase scans of the DIP:F_6TCNNQ films; schematic of a typical setup for PMIRRAS measurements; explanation of the analysis procedure of PMIRRAS data; magnifications of selected peaks in the C=C stretching and C–H bending region for DIP:F_6TCNNQ blends, and for pristine DIP selectively grown in a standing-up and lying-down configuration, respectively; DFT simulations of the isolated DIP and F_6TCNNQ molecules; FTIR and X-ray scattering data of F_6TCNNQ thin films and powder. See DOI: 10.1039/c9cp02939g

‡ Present address: ESRF The European Synchrotron, 71, Avenue des Martyrs, 38000 Grenoble, France.
§ Present address: ICMAB-CSIC, Campus de la UAB, E-08191 Bellaterra, Spain.

properties of the film[7] and the impact on its crystalline structure is much stronger than in molecular electrical doping.[8,9]

In many cases, formation of a D:A complex involves some degree of charge-transfer (CT) interactions between donor and acceptor material already in the ground-state (GS). In ref. 10, it was shown that for several TCNQ salts there is a linear relationship between the position of the highest-frequency infrared-active C≡N-stretching mode of TCNQ and the degree of fractional GS-CT of the salts, which had been estimated with independent methods. This relationship is used to trace a calibration curve for the quantification of the GS-CT degree for several other TCNQ salts. Other vibrational modes of TCNQ-derived compounds associated with hexo-cyclic C=C stretching have been shown to be sensitive to the degree of GS-CT since they are also strongly involved in the quinoid-to-benzenoid molecular deformation that accompanies the ionization process[11,12] which might result from the interaction with a donor compound. This approach based on Fourier-Transform Infrared (FTIR) spectroscopy has been used to study several other CT salts in form of macroscopic single crystals.[13–20] A prerequisite is the knowledge of the CT-affected peak position in the zero-CT/neutral and the integer-CT/ionized states, respectively.

Measurement of the GS-CT degree by means of FTIR spectroscopy, often with the aid of Density Functional Theory (DFT) calculations, has been extended to thin films of organic semiconductors. Both polymers[21–25] as well as molecular semiconductors[26–30] have been blended with other small-molecular components. Here, we investigate thin films of thickness between ~10 and 20 nm containing DIP or P3HT blended with F_6TCNNQ as D:A systems for which a driving force for GS-CT from donor to acceptor is expected according to the relative energy level alignment (Fig. 1). We use an approach which is not limited to the common analysis of the red-shift of the C≡N stretching, but extends to consider other types of vibrations, particularly C=C stretching, and their relative intensity with respect to the C≡N stretching. Interpretation of the experimental data is guided by DFT calculations on isolated F_6TCNNQ.

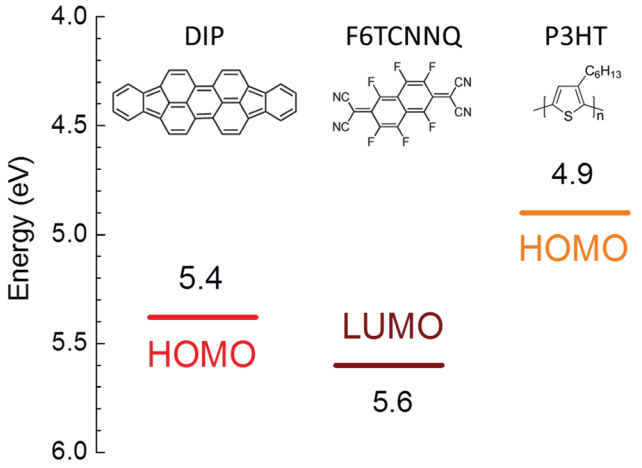

Fig. 1 Molecular structure and energy levels of the compounds used in this work. The HOMO and LUMO values were obtained from different references: HOMO of DIP from ref. 3; LUMO of F_6TCNNQ from ref. 4; HOMO of P3HT from ref. 5.

We start by characterizing the structure of DIP : F_6TCNNQ blends in different mixing ratios as a guide for the unambiguous interpretation of the FTIR-PMIRRAS spectra for this system. Next, we address effects of GS-CT interactions on the spectral shape and position of several types of vibrations for F_6TCNNQ, and we measure the amount of GS-CT in the DIP:F_6TCNNQ complex. Finally, we show a comparison between the PMIRRAS spectra for DIP:F_6TCNNQ and P3HT:F_6TCNNQ, respectively. The experimental data serve as an example to stress the importance of analyzing several types of vibrations with the support of DFT calculations in order to obtain a reliable picture of the actual strength of GS-CT interactions in these and similar D:A systems.

2 Experimental

F_6TCNNQ was purchased from Novaled. DIP was purchased from the Institut für PAH Forschung (Greifenberg, Germany). P3HT was purchased from Sigma. Si wafers covered by a ~200 nm thick Au layer were used, on which an additional Si oxide (SiO_x) layer of ~12 nm thickness has been deposited *via* Plasma-Enhanced Chemical Vapor Deposition (PECVD), similarly to ref. 31 and 32. We coated the Au substrates with SiO_x in order to prevent interaction of the molecular components with the Au surface, which might induce a change in molecular orientation[33] as well as perturb the electronic structure at the metal–organic interface.[34] Additional details on the substrate preparation and characterization are reported in the ESI.†

Thin films were grown on the Au/SiO_x substrates *via* Organic Molecular Beam Deposition (OMBD) in a vacuum chamber with a base pressure of 3×10^{-8} mbar. Prior to growth of the organic films, the substrates were cleaned first with acetone and isopropanol in an ultrasonic bath and dried under N_2. The substrates were heated up to ~500 K for 2 hours in vacuum in order to remove possible residuals of solvent.

Films of the pristine compounds as well as DIP : F_6TCNNQ mixtures in different mixing ratios were grown by co-evaporation up to a thickness around 20 nm at a substrate temperature of 300 K. The total growth rate was kept between 0.1 nm min^{-1} and 0.3 nm min^{-1} for all samples. The growth rates were monitored with two separate quartz crystal microbalances for donor and acceptor material, respectively, calibrated by X-ray reflectivity for DIP and by Atomic Force Microscopy for F_6TCNNQ both on native Si oxide, with an error on the mixing ratios of ±10%.

A pristine P3HT film as well as P3HT:F_6TCNNQ blends were prepared *via* spin coating on the Au/SiO_x substrates. Both compounds were dissolved in chloroform, where 10.4 mg P3HT and 2.3 mg of F_6TCNNQ, respectively, were added to 3.5 ml of solvent. The F_6TCNNQ solution was stirred at 55–60 °C for at least 24 hours. Two solutions in 5 : 1 P3HT : F_6TCNNQ molar ratio were prepared. The first solution was mixed 30 minutes before the spin-coating process, whereas the second was mixed 72 hours. Another solution in molar ratio 2 : 1 was prepared and mixed

30 minutes prior to spin-coating. Note that the molar ratios are defined as [moles of thiophene monomers]:[moles of F_6TCNNQ molecules]. For the thin film deposition, 50 μl of the desired solution were spin-coated at 800 rpm for 40 s, which resulted in less than 10 nm thickness of the organic films.

X-ray scattering experiments in grazing-incidence were performed at the ID10 beamline of the European Synchrotron Research Facility (ESRF, Grenoble, France).

PMIRRAS experiments were performed on a Vertex 70 infrared spectrometer equipped with a PMA 50 unit (Bruker) that allows measurements in reflection geometry. A half-wave retardation of 2200 cm^{-1} was set and the angle of incidence was 80°. Spectra were acquired with 4 cm^{-1} resolution averaging 10^3 scans, allowing the measuring chamber to be purged with dry air for 15 min prior to starting the measurement. The infrared beam is initially p-polarized by a grid polarizer (Specac) and the polarization is periodically changed between p and s with a frequency of 50 kHz by a ZnSe photoelastic modulator (Hinds Instruments). The difference between the reflectivity of the s- and p-polarized incident beam, respectively, is measured using a SR830 DSP lock-in amplifier (Stanford Instruments) and normalized by the average reflectivity.

We observe that, for our system constituted by an organic film on Au/SiO_x, the reflectance is still high and the surface selection rules for IR spectroscopy on conductive substrates maintain their general validity.[32] According to the surface selection rules, only vibrational modes that have a component of their transition dipole moment perpendicular to the metal surface can be observed.[36]

3 X-ray scattering

It is important to first analyze the structure of the thin films as a function of the DIP:F_6TCNNQ mixing ratio in order to investigate the formation of a D:A complex and possible changes in molecular orientation in the mixtures with respect to the pristine films.[8]

In Fig. 2 we show reciprocal space maps of the different DIP:F_6TCNNQ mixtures and of the pristine compounds. From Fig. 2a (pristine DIP) diffraction features stemming from the DIP thin-film phase in an upright-standing (σ) orientation can be seen, as marked by the small white circles. These features fade away and gradually disappear as the relative amount of F_6TCNNQ in the blends increases. The uniaxial alignment of the DIP crystallites in the pristine film is less pronounced than for films grown on native Si oxide,[37] an effect that can be attributed to the substrate roughness[38] (see ESI†).

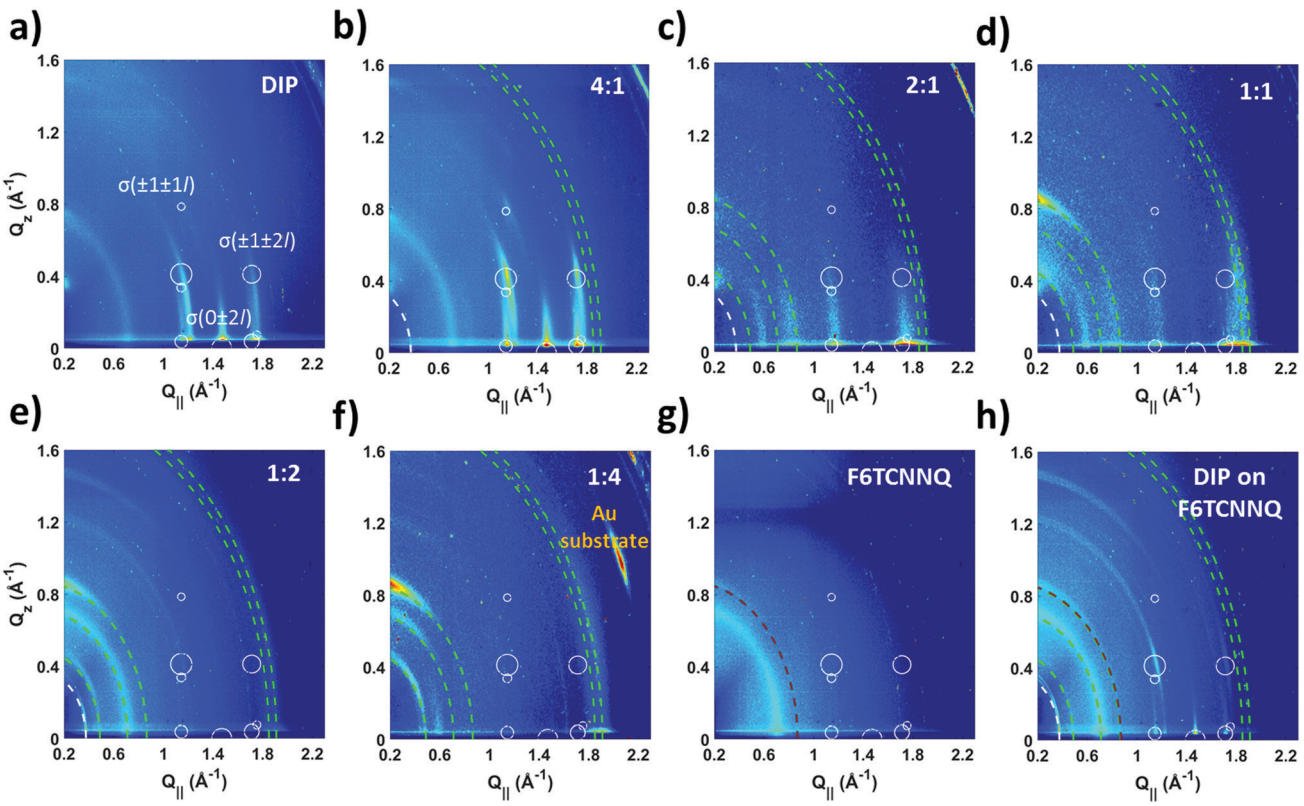

Fig. 2 Reciprocal space maps of DIP : F_6TCNNQ blends in varying mixing ratios grown on Au/SiO_x substrates. The diffraction features, that are expected to be most intense for the thin film phase of DIP in σ-orientation, are indicated as white circles with a diameter proportional to the intensity. For pristine DIP, Miller indexes of the corresponding truncation rods according to ref. 35 are shown. The dashed curved lines indicate specific diffraction features as follows: white, (001) Bragg peak for the DIP thin film polymorph; brown, pristine F_6TCNNQ; green, DIP:F_6TCNNQ co-crystal. The uniform diffraction ring with a total Q value of 0.71 $Å^{-1}$ comes from a Kapton window in the setup.

Going from Fig. 2b (4 : 1 mixture) to Fig. 2e (1 : 2 mixture) several observations can be made. First, it is possible to recognize a ring-like diffraction feature (white dashed circle) with $Q_{tot} \sim 0.38$ Å^{-1} corresponding to the (001) Bragg peak of randomly oriented DIP crystallites, in which a significant portion of the molecules exhibit their long molecular axis roughly parallel to the substrate surface, *i.e.* they tend to a lying-down (λ) orientation. Additionally, new diffraction features arise in the maps that we assign to the DIP:F_6TCNNQ co-crystal[39] (green dashed circles). The degree of long-range order of the co-crystal varies considerably depending on the D : A mixing ratio. In particular, the features indicating a crystalline phase become clearer only starting from the 1 : 1 film towards increasing F_6TCNNQ content.

For the 1 : 4 mixture in Fig. 2f, the diffraction features from the co-crystal are strongest. This seems to point towards a complex phase-nucleation scenario in which exceeding F_6TCNNQ is necessary to thermodynamically favor co-crystal nucleation, as it has been already observed for mixtures of organic conjugated molecules in solution.[40] The position and relative intensity of the co-crystal features correspond to our findings for this D:A system on native Si oxide,[39] in particular with the diffraction features with $Q_{\parallel} \sim 1.80$–1.95 Å^{-1} that stem from a π–π stacking distance of 3.5–3.2 Å between the conjugated cores of D and A. Therefore, a tilted edge-on orientation for the DIP:F_6TCNNQ supramolecular complex on the substrate is deduced. The DIP:F_6TCNNQ co-crystallites are overall uniaxially oriented, although with a pronounced mosaicity of $\sim\pm15°$ estimated from the intensity being spread along the Debye–Scherrer ring of the strongest co-crystal diffraction feature with $Q_{tot} \approx 0.86$ Å^{-1}. Note that the (001) diffraction ring of DIP in λ-orientation disappears due to the large molar excess of F_6TCNNQ, which hinders nucleation of a sizable amount of DIP crystallites.

In pristine F_6TCNNQ (Fig. 2g) only one weak diffraction feature with $Q_{tot} \approx 0.88$ Å^{-1} (brown dashed circle) is visible, pointing towards the coexistence of only few crystallites with amorphous domains. This feature does not match with any feature of the recently published single-crystal structure of F_6TCNNQ,[41] therefore it must stem from its thin-film phase (see ESI†). Note that this weak diffraction ring might largely overlap with the broadened spot of the co-crystal at $Q_{tot} \approx 0.86$ Å^{-1} in the mixtures with excess F_6TCNNQ. Therefore, the presence of phase-separated F_6TCNNQ domains in both crystalline and amorphous state in such mixtures seems likely.

We produced also a "planar" D:A heterointerface by depositing DIP directly on top of the F_6TCNNQ islands (this sample is denominated "DIP on F_6TCNNQ"). In contrast to blended films, this architecture allows to "artificially" obtain segregated DIP and F_6TCNNQ domains, minimizing the number of interfaces between the two materials. For this sample (Fig. 2h), DIP exhibits a more random orientation compared to the pristine film, as evidenced by the several diffraction features with nearly ring-like shape. Correspondingly, the (001) diffraction ring with $Q_{tot} \sim 0.38$ Å^{-1} is strong, and the intensity of the diffraction ring with $Q_{tot} \sim 1.5$ Å^{-1} corresponding to the (0 ±2 0) reflection of DIP becomes higher near $Q_{\parallel} \approx 0.2$ Å^{-1}. This indicates the presence of DIP domains exhibiting a nearly λ-orientation.[42] Only weak diffraction features of the co-crystal are recognizable, mainly the rings with $Q_{tot} \approx 0.48$ Å^{-1} and $Q_{tot} \approx 0.86$ Å^{-1}, the latter being probably overlapped with the stronger diffraction ring from pristine F_6TCNNQ at $Q_{tot} \approx 0.88$ Å^{-1}. We conclude that for DIP on F_6TCNNQ there are some D:A co-crystallites forming at the D:A interface but, due to the planar architecture, their relative amount is largely outweighed by the domains of the pristine compounds.

4 Infrared spectroscopy

Here we analyze FTIR-PMIRRAS spectra measured for the DIP:F_6TCNNQ blends presented above. We focus on D : A mixing ratio-dependent relative intensity changes of resonance peaks and their shifts. We discuss such observations in terms of three distinct factors. First, we point out the effect of molecular orientation. Second, we consider the effect of GS-CT interactions between DIP and F_6TCNNQ. Third, we take into account solvent-shifts. We divide the discussion between two spectral ranges. First we analyze the range ~1350–1700 cm^{-1} where the strongest vibrations are found that include C=C stretching for both molecules, and also in-plane C–H bending for DIP. Secondly, we analyze the range ~2180–2240 cm^{-1} where the C≡N stretching modes for F_6TCNNQ are found.

Subsequently, we analyze the C≡N stretching region for F_6TCNNQ in mixtures with P3HT and, finally, we give an overview of the spectra for P3HT:F_6TCNNQ mixtures in the full range from ~1350 cm^{-1} to ~2250 cm^{-1}.

4.1 C=C stretching region in DIP:F_6TCNNQ

The PMIRRAS spectra are shown in Fig. 3 for the region 1300–1750 cm^{-1}, where vibrational modes are located that include C=C stretching and C–H in-plane bending for DIP

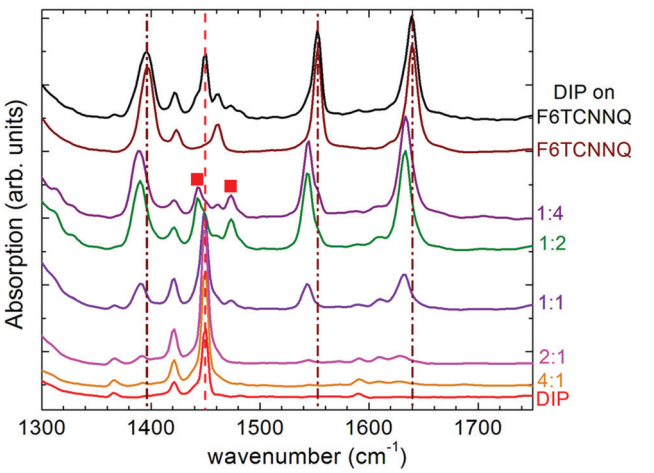

Fig. 3 PMIRRAS spectra of DIP:F_6TCNNQ mixed films and pristine compounds in the region of the skeletal C=C stretching and in-plane C–H bending modes. The brown (red) vertical lines mark the strongest modes of pristine F_6TCNNQ (DIP) at 1396.5, 1553 and 1640 (1449.5) cm^{-1}. The red squares mark two modes stemming from DIP in a more lying-down configuration.

and endo- and hexo-skeletal C=C stretching for F_6TCNNQ. Starting from pristine DIP, the spectra gradually change into the spectrum of pristine F_6TCNNQ, which qualitatively confirms the nominal mixing ratios.

The strongest resonance of DIP is located at 1449.5 cm^{-1} and is marked in Fig. 3 by a vertical dashed red line. According to our DFT calculations (see ESI†), this breathing mode has B_{1u} parity and consists only marginally of C=C stretching vibrations of the DIP skeleton; indeed it features mostly in-plane C–H bending of the hydrogen atoms located on the indeno-groups, and has a transition dipole moment (TDM) parallel to the long molecular axis. The weak low-energy shoulder of this peak at 1442.0 cm^{-1} in pristine DIP is not expected from DFT calculations and is therefore attributed to a Davydov splitting of the strongest DIP mode at 1449.5 cm^{-1}. For the 1 : 2, 1 : 4 and DIP on F_6TCNNQ samples, this shoulder substantially gains oscillator strength relative to the component at 1449.5 cm^{-1}. Also, in these mixtures an additional peak at 1474.0 cm^{-1} appears with its shoulder at 1482.5 cm^{-1}. Both features are predicted by DFT and mostly involve in-plane C–H bending of the bonds located on the indeno-groups as well as on the perylene core.

The low-energy Davydov component of the strongest DIP mode at 1449.5 cm^{-1} and the additional peak at 1474.0 cm^{-1} are marked by a red square in Fig. 3. These features become stronger relative to the others in the mixtures with F_6TCNNQ due to a change in the average orientation of the DIP molecules (see ESI†). In the blended films, DIP is embedded either in pristine crystallites or in D:A co-crystallites with F_6TCNNQ. From the X-ray scattering data in Fig. 2 we have seen that the pristine DIP crystallites undergo an orientational transition, with a sizable portion of DIP molecules exhibiting a nearly λ-orientation. For the DIP molecules embedded in the co-crystal unit cell, a possible edge-on configuration with a pronounced tilting towards the substrate[39] together with the mosaicity of the co-crystallites (Fig. 2f) imply that a high portion of DIP is oriented roughly parallel to the substrate surface. These scenarios, together with the surface selection rules for IR spectroscopy in reflection geometry on conductive substrates, can fully explain the changes in relative intensities of the DIP vibrational modes discussed above.

An important observation from Fig. 3 is the red-shift of the strongest F_6TCNNQ modes when going from pristine F_6TCNNQ (or DIP on F_6TCNNQ) to the bulk heterojunctions. The weaker peaks at 1424 cm^{-1} and 1461 cm^{-1} in pristine F_6TCNNQ do not shift significantly in the bulk mixtures, with the former peak almost overlapping with a resonance of DIP. This red-shift of the strongest F_6TCNNQ resonances is attributed to GS-CT interactions in the DIP:F6TCNNQ co-crystal. The position of these peaks (Table 1) varies only slightly in the mixtures because some amount of co-crystal is always present, but the environment surrounding each crystallite changes slightly depending on the mixing ratio. We recall that, for the mixed films, the presence of D:A co-crystallites is evidenced by X-ray diffraction (Fig. 2b–f).

In F_4TCNQ single crystals, the hexo-skeletal C=C stretching is heavily affected by GS-CT interactions.[12] For F_6TCNNQ, our DFT calculations suggest a different scenario. The three strongest modes indicated above at 1396.5 cm^{-1}, 1553 cm^{-1} and 1640 cm^{-1} are mostly constituted by endo-skeletal C=C stretching vibrations (see ESI†). The biggest contribution of the hexo-skeletal C=C bond is found for the excitation of the mode at 1553 cm^{-1} in pristine F_6TCNNQ, which exhibits the largest CT-induced red-shift. Therefore, though in F_4TCNQ mostly the hexo-skeletal C=C stretching is affected, in F_6TCNNQ also the endo-skeletal C=C bonds are heavily affected by GS-CT interactions. This might indicate a more effective charge delocalization in the extended quinoid system of F_6TCNNQ compared to the smaller F_4TCNQ.

Table 1 Position of F_6TCNNQ FTIR peaks in the pristine film and in the mixtures, the latter expressed as DIP : F_6TCNNQ molar ratio. All peak positions given in cm^{-1}

F_6TCNNQ	1 : 4	1 : 2	1 : 1	2 : 1	4 : 1
1553.0	1544.0	1544.0	1543.5	1544.0	1545.5
1640.0	1633.5	1633.5	1632.5	1629.0	1628.0
1396.5	1389.5	1390.0	1391.0	1391.0	1392.0

A closer inspection of the data in Fig. 3 reveals a high-energy shoulder of the red-shifted F_6TCNNQ modes in the bulk mixtures (see ESI†). This shoulder originates from phase-separated F_6TCNNQ domains and therefore resembles the position of the vibrations unaffected by GS-CT. As noted above, exceeding F_6TCNNQ seems to favor nucleation of the co-crystal. Since thin film growth is a non-equilibrium process, nucleation of the co-crystal might be partly suppressed if the amount of F_6TCNNQ is insufficient. Therefore, spectral features of phase-separated F_6TCNNQ are also observed in the mixtures with excess DIP. The presence of pristine F_6TCNNQ domains in these mixtures seems confirmed by the analysis of film morphology from AFM scans in phase-sensitive mode (see ESI†).

Inspecting the data for the DIP on F_6TCNNQ sample more closely in Fig. 3 reveals the presence of a weak, low-energy shoulder for some of the strongest C=C stretching modes (see ESI†). This shoulder stems from GS-CT interactions within the relatively small amount of D:A co-crystal formed at the interface between F_6TCNNQ islands and DIP coating, in agreement with the results from X-ray scattering (Fig. 2h).

4.2 C≡N stretching region in DIP:F_6TCNNQ

In Fig. 4a the spectral region 2170–2255 cm^{-1} is shown, where the C≡N stretching modes are located. Pristine DIP obviously does not exhibit this type of vibration. Overall, four peaks are observed, which are numbered in decreasing energy. Already by qualitative inspection of Fig. 4, a gradual red-shift of these modes as a function of D : A mixing ratio is evident. We fitted peaks 1–4 with a sum of Lorentzian curves in order to accurately determine their position (see ESI†). In the following, we first consider the attribution of these four peaks in detail, then we provide an estimate for the degree of GS-CT in the DIP : F_6TCNNQ complex.

4.2.1 Peak assignment. DFT calculations for the isolated F_6TCNNQ molecule predict only two antisymmetric C≡N stretching modes (see ESI†). However, the spectrum of the

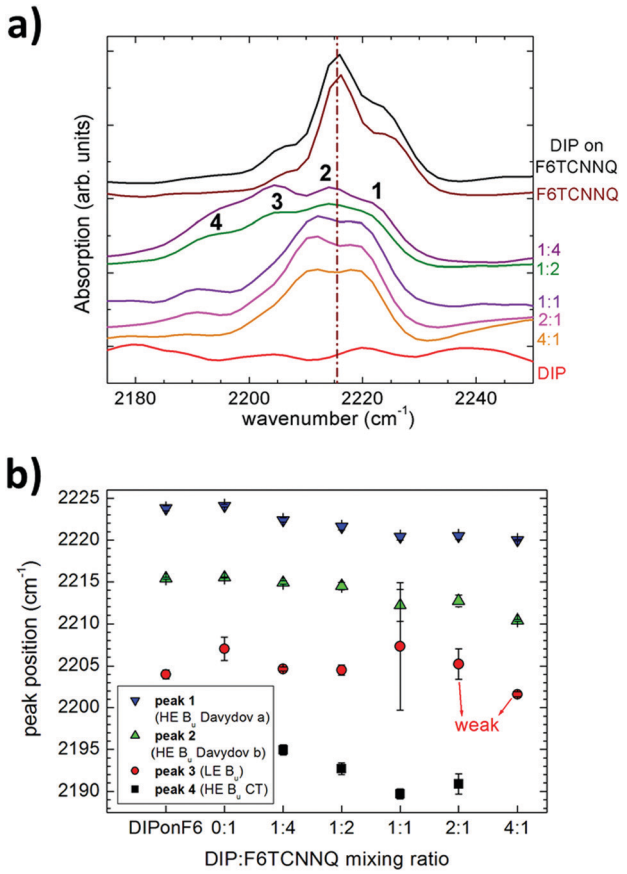

Fig. 4 (a) PMIRRAS spectra of DIP:F_6TCNNQ mixtures and pristine compounds in the region of the C≡N stretching modes. The vertical dash-dotted line marks 2215.5 cm^{-1}, which corresponds to the strongest Davydov component of the high energy B_u mode in pristine F_6TCNNQ. The data have been scaled for better comparability. The resolution of the spectra is 2 cm^{-1}. (b) Fitted C≡N stretching peak positions. The error bars represent the statistical error of the fits. Abbreviations in the legend based on the DFT calculations for the single molecule: peak 1, Davydov component "a" of the high-energy (HE) B_u mode; peak 2, Davydov component "b" of the HE B_u mode; peak 3, low-energy (LE) B_u mode; peak 4, CT-affected high energy B_u mode.

pristine material shows three peaks, as already noticed in ref. 24. Based on our DFT calculations, we suggest that peak 1 and 2 are the Davydov components of the stronger high energy mode of B_u symmetry, whereas peak 3 is the weaker, low energy B_u mode. This interpretation is supported by considering the peak distance and width. Peak 1 and 2 are ~7 cm^{-1} apart from each other, and their average position is ~13 cm^{-1} apart from peak 3. This indicates the "finer" character of the Davydov splitting compared to the energy separation between the two modes. Additionally, peak 1 and 2 have similar width for all mixtures.

The change in relative peak intensity of peaks 1–3 as a function of D : A mixing ratio can be explained in terms of orientation change of the F_6TCNNQ molecules when pristine F_6TCNNQ crystallites coexist with DIP:F_6TCNNQ co-crystals. Our DFT calculations show that the two IR-active C≡N stretching modes in the isolated molecule have their respective transition dipole moment perpendicular to each other (see ESI†). Therefore, their relative intensity can be very sensitive to changes in molecular orientation. This effect is similar to what is observed for the C–H in-plane bending modes of DIP (Fig. 3). As noted above, segregated F_6TCNNQ domains can be present even in the mixtures with excess DIP due to both thermodynamic and kinetic factors.

Peak 4 is assigned to the B_u mode, which is red-shifted as a consequence of GS-CT interactions between DIP and F_6TCNNQ within the supramolecular D:A complex. In our case, we assume that we are able to sensibly detect only the strongest CT-affected B_u mode. The intensity of peak 4 *vs.* DIP : F_6TCNNQ mixing ratio matches the trend of the intensity of the X-ray diffraction features for the D:A co-crystal (Fig. 2b–f), which supports the assignment.

4.2.2 Evaluation of the GS-CT degree. In Fig. 4b, the peak positions as a function of mixing ratio are shown. Overall, one can see that peak 1 and 2 exhibit a rather monotonic red-shift with increasing DIP content, with their position changing by ~5 cm^{-1} at most. The CT-affected peak 4 also exhibits a more or less monotonic red-shift as a function of film composition by ~5 cm^{-1} as well. We attribute these shifts to the gradual change of the local molecular environment surrounding either F_6TCNNQ domains (peak 1 and 2) or DIP:F_6TCNNQ co-crystallites (peak 4). Since the crystals are much smaller than the wavelength, an effective medium approximation[43] can be applied for the mixtures of varying D : A ratio, which leads to a solvent-shift. Note that peak 3 does not exhibit a clear trend with film composition.

Mode-shifting due to the dielectric properties of the medium affects also the C=C stretching region (see ESI†), but we do not carry out any quantitative analysis using the resonances of this region. Nevertheless, we mention that it was noticed in the literature[12,44] that the cyano-wings in F_4TCNQ are more exposed than the backbone to influences from the surrounding molecular environment.

Due to the observed mixing ratio-dependent position of peak 1, 2 and 4, we report two different numbers to quantify the amount of GS-CT. The first one is calculated by taking the shift between the CT-affected and the unaffected mode in the DIP : F_6TCNNQ 1 : 1 mixture. The other is determined by taking the unaffected mode in the pristine F_6TCNNQ film as reference. The position of the unaffected mode for both films is calculated by taking the intensity-weighted average position of the Davydov components, peak 1 and peak 2 (Fig. 4a).

The intensity ratio I_{p1}/I_{p2} of the Davydov components of the high-energy B_u C≡N stretching mode is ~1/1 for the 1 : 1 mixture and ~1/2 for pristine F_6TCNNQ. Thus, the reference position for the zero-CT state, ν_0, is (2216.3 ± 1.2) cm^{-1} for the 1 : 1 mixture and (2218.4 ± 0.1) cm^{-1} for pristine F_6TCNNQ (Fig. 4b and Table S2 in the ESI†). The position of the CT-affected mode peak 4 in the 1 : 1 mixture, ν_{CT}, is (2189.7 ± 0.6) cm^{-1}. The experimentally observed CT-induced red-shift, $\nu_0 - \nu_{CT} \equiv \Delta\nu_{CT,exp}$, is therefore (26.6 ± 1.8) cm^{-1} and (28.7 ± 0.7) cm^{-1} when referred to the 1 : 1 mixture and to pristine F_6TCNNQ, respectively.

Our DFT calculations predict a red-shift, $\Delta\nu_{CT,full}$, of 33.0 cm^{-1} for the stronger B_u mode when going from the isolated neutral F_6TCNNQ to its mono-anion (see ESI†). This value is

comparable to the 31.3 cm^{-1} observed experimentally for the case of integer-type GS-CT from the donor dibenzotetrathiafulvalene (DBTTF) to F_6TCNNQ,[45] but it is smaller than the ~37 cm^{-1} calculated by DFT in ref. 24. Assuming a simple linear relationship between the amount of red-shift and the degree of CT,[10] we calculate a partial CT $\rho = \Delta\nu_{CT,exp}/\Delta\nu_{CT,full}$ of (0.81 ± 0.06) *e* and (0.87 ± 0.02) *e* referred to the 1 : 1 mixture and to pristine F_6TCNNQ, respectively. As average value one therefore obtains (ρ_{avg} = 0.84 ± 0.04) *e*. This value is significantly higher than the 0.62 *e* estimated by means of FTIR for a DBTTF:F_6TCNNQ complex, in spite of the fact that F_6TCNNQ is a stronger acceptor for DBTTF than for DIP.[45] Note that the coexistence of such DBTTF:F_6TCNNQ CT complex with the fully ionized donor and acceptor species has also been suggested.[45] In general, the parameters relating the formation of a D:A complex with the corresponding degree of CT occurring in the ground state are numerous and their contributions not trivial to isolate. Apart from the mere HOMO(D)–LUMO(A) energy difference, other factors like crystal structure[17] and orbital overlap and symmetry[29,46] need to be considered. In particular, many D:A pairs of planar OSCs show the tendency to form supramolecular complexes for which orbital hybridization and strong electronic coupling plays an important role in determining partial CT, as it has been well documented in ref. 45 and 47. For the system constituted by DIP:F6TCNNQ studied here, orbital hybridization within the D:A complex was also suggested by us to explain the lowest-energy electronic transition in the co-crystal.[39]

To summarize for this system, using two different values as reference for the zero-CT state allows to take into account the systematic peak shifts with D : A mixing ratio and to provide an estimation of the deviations in ρ. Overall, it is possible to say that the supramolecular complex formed by DIP and F_6TCNNQ belongs to the class of compounds exhibiting a high degree of partial GS-CT.

4.3 P3HT:F_6TCNNQ blends

For comparison, we consider now P3HT (Fig. 1) as donor for F_6TCNNQ as recently introduced in ref. 24. We divide the results and discussion into two sections dedicated, respectively, to the analysis of the C≡N stretching region alone and to the parallel analysis of the C≡N and C=C stretching regions.

4.3.1 C≡N stretching region. In order to deepen the study of this interesting D:A system,[24] we show in Fig. 5 a comparison between the PMIRRAS spectra in the C≡N stretching region for pristine F_6TCNNQ, DIP : F_6TCNNQ 1 : 1 and P3HT:F_6TCNNQ blends in different mixing ratios and preparation times.

In P3HT:F_6TCNNQ there is barely any trace of peak 1–3 of the pristine acceptor. The solution mixing seems therefore effective in dissolving the F_6TCNNQ molecules between the polymer chains without leaving F_6TCNNQ aggregates, as it is also confirmed by the increasing peak sharpness with longer mixing time for the 5 : 1 mixtures.

The strongest peak for the C≡N stretching in all P3HT:F_6TCNNQ blends measured is located at 2194 cm^{-1}. The same uncertainty in peak position obtained for DIP:F_6TCNNQ mixtures

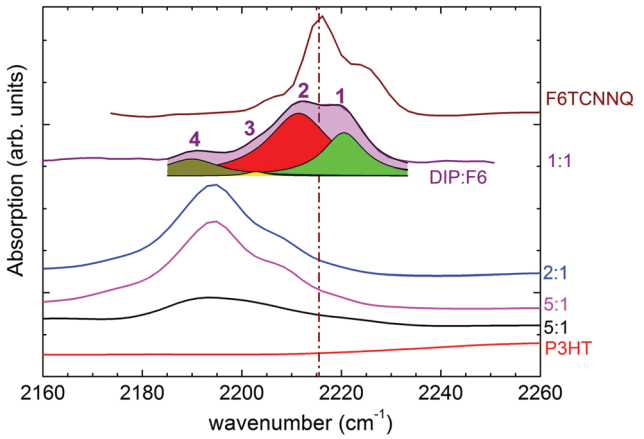

Fig. 5 PMIRRAS spectra of DIP : F_6TCNNQ 1 : 1 blend, P3HT:F_6TCNNQ blends and pristine F_6TCNNQ and P3HT in the C≡N stretching region. For the DIP : F_6TCNNQ 1 : 1 blend, the same peak numbering as in Fig. 4 has been adopted, and the multi-peak Lorentzian fit is shown. The P3HT : F_6TCNNQ blends in different molar ratios have been spin-coated from solutions mixed for different amounts of time: 5 : 1 (black curve), 30 min; 5 : 1 (magenta curve), 72 h; 2 : 1, 30 min. The vertical dash-dotted line marks 2215.5 cm^{-1}, which corresponds to the strongest Davydov component of the high-energy B_u mode in pristine F_6TCNNQ.

can been assumed for the P3HT:F_6TCNNQ mixtures. The high-energy shoulder of the peak at 2194 cm^{-1} in the mixtures might originate from different relative configurations of the complex formed locally by P3HT and F_6TCNNQ.[48] Here, the most important finding is that the CT-affected C≡N stretching mode in P3HT:F_6TCNNQ lies approximately at the same position as the CT peak in DIP:F_6TCNNQ with no significant differences.

By the mere comparison of the C≡N stretching modes the conclusion would be that CT interactions in the two systems have very similar strength. However, the UV-vis-NIR absorption measurements in ref. 24 clearly show the presence of the ionic species of both donor and acceptor for P3HT:F_6TCNNQ, namely: (a) the two relatively sharp peaks at ~980 nm (~1.27 eV) and ~1150 nm (~1.08 eV), signatures of F_6TCNNQ in the mono-anionic state,[4] (b) the broad polaronic band of the P3HT cation with onset around 1300 nm (~0.95 eV) and extending in the NIR.[49] For DIP:F_6TCNNQ, instead, no clear signatures of the F_6TCNNQ anion could be identified.[39] Therefore, two different scenarios are suggested. For DIP:F_6TCNNQ, the data point towards the formation of a supramolecular complex with partial GS-CT, whereas for P3HT:F_6TCNNQ integer GS-CT with formation of polaronic species of donor and acceptor is most likely. An integer GS-CT picture in P3HT:F_6TCNNQ is further supported by the established full ionization of donor and acceptor in F_4TCNQ-doped P3HT[49] since F_6TCNNQ is an acceptor even stronger than F_4TCNQ.

Overall, we conclude that the shift of the C≡N stretching modes alone does not give conclusive information about the nature of GS-CT interactions in P3HT:F_6TCNNQ.

4.3.2 Comparison between C=C and C≡N stretching region. In order to complement the information on P3HT:F_6TCNNQ, full-range PMIRRAS spectra are shown in Fig. 6 for the same samples as in Fig. 5.

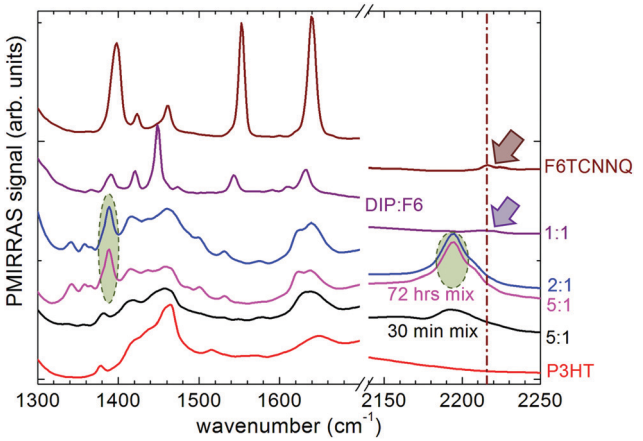

Fig. 6 PMIRRAS spectra of DIP : F_6TCNNQ 1 : 1 blend, P3HT:F_6TCNNQ blends and pristine F_6TCNNQ and P3HT. Note the different scale before and after the break along the abscissa axis. The vertical dash-dotted line marks 2215.5 cm^{-1}. The arrows point to the C≡N stretching modes for DIP : F_6TCNNQ 1 : 1 and pristine F_6TCNNQ, which appear as tiny features relative to the much stronger C=C stretching modes in the fingerprint region. The green circles highlight F_6TCNNQ modes which are predicted by DFT calculations to have very similar oscillator strength in the mono-anion.

For the P3HT:F_6TCNNQ blends, assignment of the peaks to either the donor polymer or the acceptor in the C=C stretching region is not as straightforward as in DIP:F_6TCNNQ. Here, we rather intend to stress the remarkable change in intensity of the C≡N stretching features relative to the C=C stretching features for the two systems DIP:F_6TCNNQ and P3HT:F_6TCNNQ, respectively. For the mixtures containing DIP as donor, the C≡N stretching modes exhibit a much lower cross-section relative to the C=C stretching modes, whereas in the polymeric system their relative intensity is similar. Such an effect is clearly not related to changes in molecular orientation of the F_6TCNNQ units. Indeed, the mosaicity of locally ordered P3HT chains doped with F_4TCNQ[48] is similar to that of the DIP:F_6TCNNQ co-crystals (Fig. 2) observed here.

Our DFT calculations performed on the isolated F_6TCNNQ molecule (see ESI†) show that the intensity of the resonances in the C=C stretching region relative to those in the C≡N stretching region is much higher for the neutral F_6TCNNQ than for its mono-anion. For the P3HT : F_6TCNNQ 2 : 1 mixture and in the 5 : 1 mixture with longer mixing time, we recognize the intense peak at ~1389 cm^{-1} as the strongest C=C stretching mode of the F_6TCNNQ mono-anion. Its oscillator strength is very similar to that of the strongest C≡N stretching mode (green circles in Fig. 6), in full agreement with the DFT calculations for the F_6TCNNQ mono-anion. These observations further support the conclusion that CT from P3HT to F_6TCNNQ occurs in the GS *via* donation of a full electron and formation of polaronic species.

DIP:F_6TCNNQ is therefore a system for which a relatively strong GS-CT is observed, but the spectral features associated with the ionic species are not observed. Assuming for both D:A systems an energetically favored electron-donation from the donor to the acceptor (Fig. 1), the different kinds of CT, respectively, might be explained by the superior ability of P3HT to relax the positive counterpart of the generated polaron *via* charge delocalization along the polymeric backbone.[50,51]

The difficulty to obtain a reliable picture of the actual strength of GS-CT interactions in P3HT:F_6TCNNQ from the C≡N stretching modes alone can be rationalized as follows. On the one hand, the impact of a full GS-CT on a given set of vibrational modes will depend on where the negative charge acquired by the acceptor is most likely localized. On the other hand, the two kinds of vibrations in F_6TCNNQ, *i.e.* C=C and C≡N stretching, could be affected differently by GS-CT interactions depending on the solid state packing of the acceptor, which in one case is embedded in the co-crystal with DIP and in the other case in the polymer chains. For example, short (donor)C–H···N≡C(F_6TCNNQ) contacts[20] more than the π-stacking might affect C≡N stretching modes, whereas intermolecular D:A coupling, therefore also GS-CT coupling, occurs mainly *via* the π-stacking.

5 Conclusions

In conclusion, we have carried out a study of ground-state charge-transfer interactions by means of FTIR spectroscopy for two representative D:A systems where F6TCNNQ is used as acceptor for the donors DIP and P3HT, respectively.

For DIP:F6TCNNQ blended films, a preliminary characterization of film structure by means of X-ray scattering provides a solid guide for the interpretation of FTIR-PMIRRAS spectra. Inspection of the C=C stretching C–H in-plane bending region in DIP:F_6TCNNQ blends reveals: (a) the effect of changes in molecular orientation on the relative intensity of the Davydov components of the strongest DIP mode and (b) red shifts of up to 10 cm^{-1} of the strongest F_6TCNNQ modes involving mostly endo-skeletal bonds. Such shifts are related to the formation of a DIP:F_6TCNNQ supramolecular complex and to GS-CT interactions. Together with D:A co-crystallites, traces of phase-separated F_6TCNNQ are detected in all the blends.

In the C≡N stretching region, for DIP:F_6TCNNQ we unambiguously identify one red-shifted mode due to GS-CT, together with three other modes stemming from pristine F_6TCNNQ, one of them being the strongest B_u mode affected by Davydov splitting. From the red-shift of the strongest, CT-affected C≡N mode with respect to the unaffected mode in the equimolar mixture with DIP and in the pristine film, respectively, we calculate an average partial CT of $\rho_{avg} = (0.84 \pm 0.04)\ e$.

For the system P3HT:F_6TCNNQ, by considering only the red-shift of the strongest C≡N stretching mode, a picture of GS-CT very similar to DIP:F_6TCNNQ emerges. However, a comparison of oscillator strength for the C=C relative to the C≡N stretching modes rather indicates stronger, integer CT-type interactions in the polymer:acceptor system. This analysis is supported by DFT calculations for the isolated F_6TCNNQ. Our conclusions agree with the available UV-vis-NIR absorption data, which show the spectral signatures of F_6TCNNQ in the mono-anionic state.

Our data evidence that, in order to draw solid conclusions about the nature of GS-CT based on vibrational spectroscopy, a

parallel analysis of the C=C and C≡N stretching regions supported by DFT calculations is required for D:A systems of OSCs featuring acceptors containing nitrile groups, therefore including some of the strongest molecular acceptors available to date.[52]

Conflicts of interest

There are no conflicts to declare.

Acknowledgements

We thank Tanja Martin (University of Tübingen) for the preparation of the SiO_x layers on Au, Ronny Löffler (University of Tübingen, $LISA^+$) for assistance during the characterization of the SiO_x layers on Au, and A. Mann (University of Tübingen) for help during the experiments. We thank Heiko Peisert and Andreas Früh (University of Tübingen) for the use of the Vertex70 FTIR spectrometer. We wish to thank Maximilian Skoda (ISIS Neutron and Muon Source) and Robert Jacobs (University of Oxford) for fruitful discussions. We thank Oleg Konovalov (ESRF, beamline ID10) for support during X-ray scattering experiments. Financial support from the DFG (project number: 239543752) is gratefully acknowledged. G. D. gratefully acknowledges support from the Carl-Zeiss-Stiftung.

References

1 K. Walzer, B. Maennig, M. Pfeiffer and K. Leo, *Chem. Rev.*, 2007, **107**, 1233–1271.
2 I. Salzmann and G. Heimel, *J. Electron Spectrosc. Relat. Phenom.*, 2015, **204**, 208–222.
3 W. Han, K. Yonezawa, R. Makino, K. Kato, A. Hinderhofer, R. Murdey, R. Shiraishi, H. Yoshida, N. Sato, N. Ueno and S. Kera, *Appl. Phys. Lett.*, 2013, **103**, 253301.
4 F. Zhang and A. Kahn, *Adv. Funct. Mater.*, 2018, **28**, 1703780.
5 I.-W. Hwang, D. Moses and A. J. Heeger, *J. Phys. Chem. C*, 2008, **112**, 4350–4354.
6 A. Hinderhofer and F. Schreiber, *Chem. Phys. Chem.*, 2012, **13**, 628–643.
7 K. Broch, U. Heinemeyer, A. Hinderhofer, F. Anger, R. Scholz, A. Gerlach and F. Schreiber, *Phys. Rev. B*, 2011, **83**, 245307.
8 A. Hinderhofer, C. Frank, T. Hosokai, A. Resta, A. Gerlach and F. Schreiber, *J. Chem. Phys.*, 2011, **134**, 104702.
9 J. P. Reinhardt, A. Hinderhofer, K. Broch, U. Heinemeyer, S. Kowarik, A. Vorobiev, A. Gerlach and F. Schreiber, *J. Phys. Chem. C*, 2012, **116**, 10917–10923.
10 J. S. Chappell, A. N. Bloch, W. A. Bryden, M. Maxfield, T. O. Poehler and D. O. Cowan, *J. Am. Chem. Soc.*, 1981, **103**, 2442–2443.
11 T. J. Emge, W. A. Bryden, F. M. Wiygul, D. O. Cowan, T. J. Kistenmacher and A. N. Bloch, *J. Chem. Phys.*, 1982, **77**, 3188–3197.
12 M. Meneghetti and C. Pecile, *J. Chem. Phys.*, 1986, **84**, 4149–4162.
13 M. Meneghetti, R. Bozio, C. Bellitto and C. Pecile, *J. Chem. Phys.*, 1988, **89**, 2704.
14 B. Mahns, O. Kataeva, D. Islamov, S. Hampel, F. Steckel, C. Hess, M. Knupfer, B. Büchner, C. Himcinschi, T. Hahn, R. Renger and J. Kortus, *Cryst. Growth Des.*, 2014, **14**, 1338–1346.
15 M. Rudloff, K. Ackermann, M. Huth, H. O. Jeschke, M. Tomic, R. Valentá, B. Wolfram, M. Bröring, M. Bolte, D. Chercka, M. Baumgarten and K. Müllen, *Phys. Chem. Chem. Phys.*, 2015, **17**, 4118–4126.
16 T. Salzillo, M. Masino, G. Kociok-Köhn, D. Di Nuzzo, E. Venuti, R. G. Della Valle, D. Vanossi, C. Fontanesi, A. Girlando, A. Brillante and E. Da Como, *Cryst. Growth Des.*, 2016, **16**, 3028–3036.
17 K. P. Goetz, J. Tsutsumi, S. Pookpanratana, J. Chen, N. S. Corbin, R. K. Behera, V. Coropceanu, C. A. Richter, C. A. Hacker, T. Hasegawa and O. D. Jurchescu, *Adv. Electron. Mater.*, 2016, **2**, 1600203.
18 P. Hu, K. Du, F. Wei, H. Jiang and C. Kloc, *Cryst. Growth Des.*, 2016, **16**, 3019–3027.
19 P. Hu, H. Li, Y. Li, H. Jiang and C. Kloc, *CrystEngComm*, 2017, **19**, 618–624.
20 P. Hu, S. Wang, A. Chaturvedi, F. Wei, X. Zhu, X. Zhang, R. Li, Y. Li, H. Jiang, Y. Long and C. Kloc, *Cryst. Growth Des.*, 2018, **18**, 1776–1785.
21 P. Pingel, L. Zhu, K. S. Park, J.-O. Vogel, S. Janietz, E.-G. Kim, J. P. Rabe, J.-L. Brédas and N. Koch, *J. Phys. Chem. Lett.*, 2010, **1**, 2037–2041.
22 F. Ghani, A. Opitz, P. Pingel, G. Heimel, I. Salzmann, J. Frisch, D. Neher, A. Tsami, U. Scherf and N. Koch, *J. Polym. Sci., Part B: Polym. Phys.*, 2015, **53**, 58–63.
23 L. Müller, D. Nanova, T. Glaser, S. Beck, A. Pucci, A. K. Kast, R. R. Schröder, E. Mankel, P. Pingel, D. Neher, W. Kowalsky and R. Lovrincic, *Chem. Mater.*, 2016, **28**, 4432–4439.
24 Y. Karpov, T. Erdmann, M. Stamm, U. Lappan, O. Guskova, M. Malanin, I. Raguzin, T. Beryozkina, V. Bakulev, F. Günther, S. Gemming, G. Seifert, M. Hambsch, S. Mannsfeld, B. Voit and A. Kiriy, *Macromolecules*, 2017, **50**, 914–926.
25 R. Fujimoto, Y. Yamashita, S. Kumagai, J. Tsurumi, A. Hinderhofer, K. Broch, F. Schreiber, S. Watanabe and J. Takeya, *J. Mater. Chem. C*, 2017, **5**, 12023–12030.
26 D. Nanova, S. Beck, A. Fuchs, T. Glaser, C. Lennartz, W. Kowalsky, A. Pucci and M. Kroeger, *Org. Electron.*, 2012, **13**, 1237–1244.
27 D. Nanova, S. Beck, M. Alt, T. Glaser, A. Pucci, K. Schultheiß, L. Dieterle, R. R. Schröder, J. Pflaum, W. Kowalsky and M. Kroeger, *Appl. Phys. A: Mater. Sci. Process.*, 2012, **112**, 1019–1025.
28 H. Méndez, G. Heimel, S. Winkler, J. Frisch, A. Opitz, K. Sauer, B. Wegner, M. Oehzelt, C. Röthel, S. Duhm, D. Többens, N. Koch and I. Salzmann, *Nat. Commun.*, 2015, **6**, 8560.
29 Q. Zhang, X. Liu, F. Jiao, S. Braun, M. J. Jafari, X. Crispin, T. Ederth and M. Fahlman, *J. Mater. Chem. C*, 2017, **5**, 275–281.
30 V. Belova, P. Beyer, E. Meister, T. Linderl, M.-U. Halbich, M. Gerhard, S. Schmidt, T. Zechel, T. Meisel, A. V. Generalov,

A. S. Anselmo, R. Scholz, O. Konovalov, A. Gerlach, M. Koch, A. Hinderhofer, A. Opitz, W. Brütting and F. Schreiber, *J. Am. Chem. Soc.*, 2017, **139**, 8474–8486.
31 S. Szunerits and R. Boukherroub, *Langmuir*, 2006, **22**, 1660–1663.
32 I. Zawisza, G. Wittstock, R. Boukherroub and S. Szunerits, *Langmuir*, 2007, **23**, 9303–9309.
33 A. C. Dürr, N. Koch, M. Kelsch, A. Rühm, J. Ghijsen, R. L. Johnson, J.-J. Pireaux, J. Schwartz, F. Schreiber, H. Dosch and A. Kahn, *Phys. Rev. B*, 2003, **68**, 115428.
34 L. Romaner, G. Heimel, J. L. Brédas, A. Gerlach, F. Schreiber, R. L. Johnson, J. Zegenhagen, S. Duhm, N. Koch and E. Zojer, *Phys. Rev. Lett.*, 2007, **99**, 256801.
35 M. A. Heinrich, J. Pflaum, A. K. Tripathi, W. Frey, M. L. Steigerwald and T. Siegrist, *J. Phys. Chem. C*, 2007, **111**, 18878–18881.
36 M. W. A. Skoda, PhD thesis, Wadham College, Oxford, 2007.
37 S. Kowarik, A. Gerlach, S. Sellner, L. Cavalcanti, O. Konovalov and F. Schreiber, *Appl. Phys. A*, 2009, **95**, 233–239.
38 H. Peisert, I. Biswas, L. Zhang, M. Knupfer, M. Hanack, D. Dini, D. Batchelor and T. Chassé, *Surf. Sci.*, 2006, **600**, 4024–4029.
39 G. Duva, L. Pithan, C. Zeiser, B. Reisz, J. Dieterle, B. Hofferberth, P. Beyer, L. Bogula, A. Opitz, S. Kowarik, A. Hinderhofer, A. Gerlach and F. Schreiber, *J. Phys. Chem. C*, 2018, **122**, 18705–18714.
40 J. H. ter Horst and P. W. Cains, *Cryst. Growth Des.*, 2008, **8**, 2537–2542.
41 J. Li, I. Duchemin, O. M. Roscioni, P. Friederich, M. Anderson, E. Da Como, G. Kociok-Köhn, W. Wenzel, C. Zannoni, D. Beljonne, X. Blase and G. D'Avino, *Mater. Horiz.*, 2018, **6**, 107–114.
42 G. Duva, A. Mann, L. Pithan, P. Beyer, J. Hagenlocher, A. Gerlach, A. Hinderhofer and F. Schreiber, *J. Phys. Chem. Lett.*, 2019, **10**, 1031–1036.
43 H. Tompkins and E. A. Irene, *Handbook of ellipsometry*, William Andrew, Norwich, NY, 2005, vol. XII, p. 891.
44 A. Morherr, S. Witt, A. Chernenkaya, J.-P. Bäcker, G. Schönhense, M. Bolte and C. Krellner, *Phys. B*, 2016, **496**, 98–105.
45 P. Beyer, D. Pham, C. Peter, N. Koch, E. Meister, W. Brütting, L. Grubert, S. Hecht, D. Nabok, C. Cocchi, C. Draxl and A. Opitz, *Chem. Mater.*, 2019, **31**, 1237–1249.
46 E. Kampar and O. Neilands, *Russ. Chem. Rev.*, 1986, **55**, 334–342.
47 I. Salzmann, G. Heimel, S. Duhm, M. Oehzelt, P. Pingel, B. George, A. Schnegg, K. Lips, R.-P. Blum, A. Vollmer and N. Koch, *Phys. Rev. Lett.*, 2012, **108**, 035502.
48 D. T. Duong, C. Wang, E. Antono, M. F. Toney and A. Salleo, *Org. Electron.*, 2013, **14**, 1330–1336.
49 P. Pingel and D. Neher, *Phys. Rev. B*, 2013, **87**, 115209.
50 M. Zamadar, S. Asaoka, D. C. Grills and J. R. Miller, *Nat. Commun.*, 2013, **4**, 2818.
51 A. M. Valencia and C. Cocchi, *J. Phys. Chem. C*, 2019, **123**, 9617–9623.
52 I. E. Jacobs and A. J. Moulé, *Adv. Mater.*, 2017, **29**, 1703063.